Published on Mar 28, 2023 by Arcadia Science **DOI**: 10.57844/arcadia-fh8f-xz51

Inducing protoplast formation in *Phaeodactylum tricornutum* by silica deprivation, enzymatic treatment, or cytoskeletal inhibition

Treating *P. tricornutum* cells with serine endopeptidases or certain cytoskeletal inhibitors induces the formation of cell wall-free protoplasts and suggests a novel role for actin and myosin in preventing protoplast formation.

Contributors (A-Z)

Prachee Avasthi, Brae M. Bigge, Megan L. Hochstrasser, Cameron Dale MacQuarrie, Atanas Radkov

Version 1 · Mar 31, 2025

Purpose

The algal diatom species *Phaeodactylum tricornutum* has three distinct morphotypes. We sought to investigate morphological determinants in these unique diatoms.

Enzymatic cell wall disruption and cell wall weakening by omitting silica from the media led cells to “pop out” and persist as round protoplasts. We have thoughts on probable mechanisms underlying these observations, but will leave these for others to explore.

We also share results that treatments with cytoskeletal inhibitors that target the motor protein myosin II or the branched-actin nucleating Arp2/3 complex, lead to protoplast formation. However, we’ve found these findings difficult to repeat. We share these data with the hope that others will find them useful or have ideas about what variable(s) may be changing between trials, unbeknownst to us.

- This pub is part of the **project**, “Understanding the evolution of actin-binding proteins across diverse species.” Visit the project narrative for more background and context.

Project background and goals

Diatoms are widely appreciated for their unique shapes and their silica-based cell walls. The diatom species *Phaeodactylum tricornutum* is often found in three major morphotypes: fusiform, triradiate, and ovular. In rare instances, *P. tricornutum* can adopt a more complex cruciform morphotype **[1]** or a protoplast form that lacks a cell wall **[2]** (Figure 1).

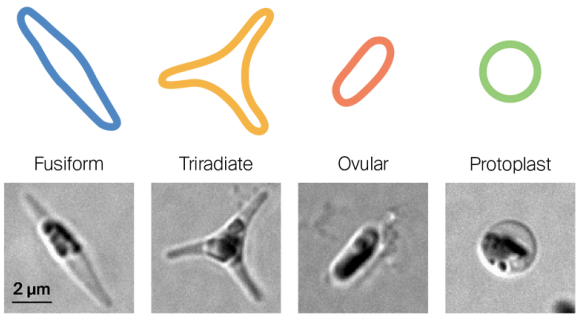

Figure 1

Morphotypes of *Phaeodactylum tricornutum*.

Representative images and corresponding cartoons of *P. tricornutum* cell morphotypes.

Mechanistic determinants of these different morphologies are murky, but we have some hints. Transcriptomic studies have revealed that *P. tricornutum* cells of different morphotypes have altered expression of several genes, including components of the actin cytoskeleton (Figure 2) **[3]**. Identifying mechanisms of actin regulation in algal species, including diatoms, is an emerging area of interest since conventional regulators atypical or missing in multiple algal species **[4][5]**. **By studying these intriguing cells, we hoped to learn how the cytoskeleton's function and regulation may differ from our canonical understanding**.

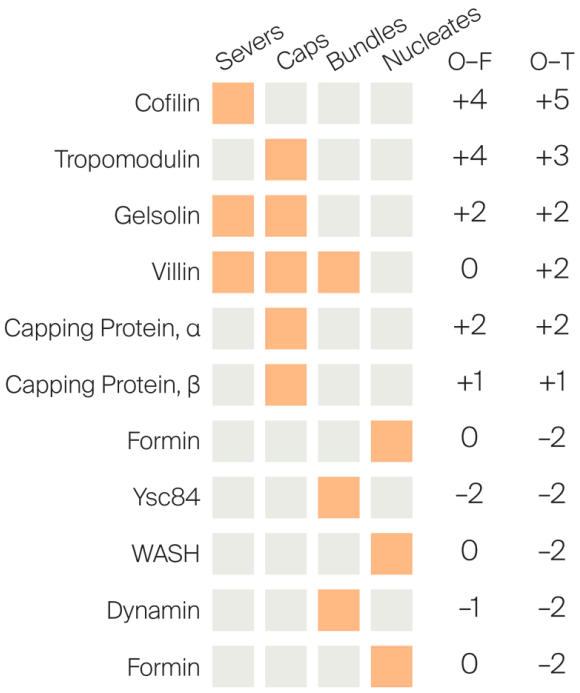

Figure 2

Comparative differential gene expression of actin-binding proteins across *P. tricornutum* morphologies from Ovide et al 2018 (CC BY 4.0).

Ovide and colleagues determined these values experimentally. O–F indicates a comparison of ovular cells to fusiform cells. O–T indicates a comparison of ovular cells to triradiate cells. A positive value indicates expression is upregulated in ovular cells and a negative value indicates expression is downregulated in ovular cells. Values indicate the RNA-seq log2 fold change.

Foundational observations of the actin cytoskeleton in *P. tricornutum*

The actin cytoskeleton plays an important role in many physiological processes across species, including cell polarity, which often dictates cell shape **[6][7][8]**. Recent work observed the *P. tricornutum* actin cytoskeleton accumulating in cortical filaments **[9] [10]**, suggesting that these rigid structures might contribute to the cell's shape. Notably, expression of actin nucleators and bundlers is lower in ovular morphotypes compared to triradiate and/or fusiform cells. Additionally, ovular cells appear to have higher expression of actin-capping proteins and F-actin-severing proteins, which limit assembly of actin filaments (Figure 2) **[3]**. This suggests that the actin cytoskeleton may be providing less structural support in ovular cells, whereas fusiform and triradiate cells benefit from more active assembly of actin filaments **[3]**. That said, ovular cells perform gliding motility **[11]**, which is actin-dependent in the similar bilaterally symmetrical pennate diatom species *Craspedostauros australis* **[12]**, so actin polymerization is playing an active role in dictating different functions between morphotypes.

Here, we explore how the actin cytoskeleton and the cell wall contribute to cell morphology in the diatom species *P. tricornutum*. Disrupting the cell wall with a peptidase or by omitting silica from the media caused cells to form round protoplasts. We were surprised to find that multiple cytoskeletal inhibitors, including an inhibitor of the motor protein myosin, also appear to disrupt the cell wall and induce protoplast formation, though we could not replicate these initial findings. We hypothesize that the actin cytoskeleton aids in the prevention of protoplast formation, possibly through anchoring the cell wall to the plasma membrane, polarized secretion of cell wall components, transcriptional regulation of cell wall biosynthetic enzymes, or through other uncharacterized means.

The approach

To understand structural contributors to diatom morphology, we disrupted the cell wall and treated *P. tricornutum* cells with a panel of actin-targeting drugs. We then imaged the cells with confocal microscopy and looked for phenotypic changes. Read detailed methods below or skip straight to the results.

Strains

Species	Strain number	Source and link	Site of isolation
Phaeodactylum tricornutum	CCMP2560	NCMA	Jericho Beach, Vancouver, British Columbia, Canada
Phaeodactylum tricornutum	CCMP2559 UTEX646	UTEX	Segelskär, Finland

Table 1. Sources for organisms studied in this pub. NCMA: National Center for Marine Algae and Microbiota, UTEX: The Culture Collection of Algae at the University of Texas at Austin.

Culturing cells

We obtained *Phaeodactylum tricornutum* cells from the Culture Collection of Algae at The University of Texas at Austin (UTEX) and the National Center for Marine Algae and Microbiota (Bigelow Laboratory) (Table 1). We selected UTEX646 and CCMP2560 strains because 95–100% of UTEX646 cells are fusiform and 80–85% of CCMP2560 cells are triradiate **[13]**, allowing us to easily study both morphotypes. We cultured cells in Guillard's F/2 medium (UTEX) in borosilicate erlenmeyer flasks, or Guillard's F/2-Si medium (Sigma-Aldrich, Cat No: G0154) in polymethylpentene erlenmeyer flasks where noted. We stored Guillard's F/2-Si medium in polypropylene reagent bottles. We grew all cells at ambient temperature under white light while in 12:12 light:dark cycles, shaking at 125 rpm.

Growth curves

We grew cells in standard Guillard's F/2 medium from UTEX, distributing 200 µL of cells across five wells on a 96-well plate. We kept the plate on an orbital shaker at 120 rpm

at room temperature under a 12:12 light:dark cycle. We measured absorbance readings using the BioTek Cytation 5 plate reader. Prior to measurement, we shook plates for 30

s. We read absorbance at 730 nm. We took readings at a normal read speed, with a 100 msec delay, providing an average reading of eight measurements per data point. We took readings every 7–18 hours over eight days (193 hours).

Microscopy

General imaging

For live differential interference contrast (DIC) imaging, we took cells from liquid culture, collected by centrifugation at 1,150 × g for 5 min, washed them in fresh Guillard's F/2 medium, and then allowed them to settle in a poly-l-lysine-coated chamber slide from Ibidi for 10 min. We then washed the wells with fresh Guillard's F/2 medium and added fresh Guillard's F/2 medium to each well prior to imaging. We acquired micrographs with a Yokogawa CSU W1-SoRa scanner unit attached to a Nikon Ti2-E confocal microscope. We acquired fluorescent images using a 100× 1.35 Plan Apo Silicone objective and acquired DIC and brightfield images using either a 100× 1.35 Plan Apo Silicone objective or a 40× 0.95 Plan Apo Air objective. We acquired Z-stacks in 0.2 µm slices using either the Ti2-zDrive or a Piezo Nano-ZDrive.

Live cell imaging

We visualized live dynamics of the actin cytoskeleton using the SPY555-FastAct dye from Spirochrome (Cat #SC205). We reconstituted lyophilized SPY555-FastAct in 50 µL anhydrous DMSO to a 1000× stock solution, in accordance with the manufacturer's protocol. We diluted stock SPY555-FastAct to 1× in fresh F/2 medium.

To visualize silica deposits, we reconstituted RatioWorks PDMPO in DMSO to 1 mM stock concentration, in accordance with the manufacturer's protocol. Stock PDMPO was diluted to a working concentration of 1 M in F/2 medium.

For both stains, *Phaeodactylum* cells were collected through centrifugation, washed in fresh F/2 medium, and resuspended in either 1× SPY555-FastAct or 1 µM RatioWorks PDMPO in F/2 medium. We incubated cells at ambient temperature while rotating and protecting them from light for 1 h prior, washed the cells in fresh F/2 medium, and imaged them as described above.

Fixed cell imaging

We visualized F-actin in fixed *P. tricornutum* cells based on previously developed methods **[9]**. We drew circles on #1.5 glass coverslips using hydrophobic PAP pens. We added 100 µL of poly-l-lysine to the center of the circle for 15 min at ambient temperature before washing coverslips in water. We placed 200 µL of *P. tricornutum* cells in the center of the coverslip and left for 10 min at room temperature to allow cells to adhere. After removing excess cells and medium, we fixed cells for 1 h in the dark at ambient temperature with 200 µL of 4% paraformaldehyde (PFA) in 10 mM HEPES, pH 7.4. Next, we washed cells in PBS for 5 min. We then permeabilized cells for 3 min in the dark at ambient temperature using diatom permeabilization buffer (DPB) (1% bovine serum albumin, 0.1% Triton X-100, PBS). Attempts to permeabilize *P. tricornutum* cells in acetone at –20 °C resulted in cells exploding. We removed excess DPB and replaced it with 100 µL of 125 nM phalloidin-Atto 488 and incubated at ambient temperature in the dark for 30 min. We then washed cells in PBS for 5 min. In some experiments, we then costained coverslips with 3 µM DAPI for 5 min at ambient temperature in the dark before washing again for 5 min. We left coverslips to dry in the dark at ambient temperature before mounting on a standard microscope slide with 7 µL Fluoromount G. We kept samples at 4 °C prior to imaging.

Cytoskeletal drug treatments

Cell wall degradation

We treated *P. tricornutum* cells with 0.3 Anson units of Subtilisin A protease, isolated from *Bacillus licheniformis* (Alcalase enzyme, Sigma-Aldrich Cat. #126741) per mL of media in 1.5 mL tubes for 1 h (or 2 h where noted) while rotating. We then collected cells by centrifugation at 1,150 × g for 5 min and washed them in fresh medium prior to imaging.

Drug treatments

We collected cells from culture at 1,150 × g for 5 min and washed them in fresh Guillard's F/2 medium (without silica where noted) twice. We then treated cells with the specified concentration of cytoskeletal drugs for 2 h in 1.5 mL tubes on a tube rotator

in the dark. We collected cells at 1,150 × g for 5 min, washed in fresh F/2 medium, and then fixed in 4% paraformaldehyde for 30 min prior to imaging.

Image analysis

We processed and analyzed all imaging data using FIJI software (NIH). We counted morphology percentages manually using the FIJI Cell Counter plugin.

Modeling and docking

Below are the 10 myosin proteins and six actin-like proteins from *P. tricornutum*, and their corresponding accession numbers on GenBank or UniProt, that we used in our analysis (Table 2).

Name	**Accession number**
Myosins	*GenBank accession*
PtMyo29	GQ141540 - ACS35536.1
PtMyoA	GQ141541 - ACS35537.1
PtMyoB	GQ141542 - ACS35538.1
PtMyoC	GQ141543 - ACS35539.1
PtMyoD	GQ141544 - ACS35540.1
PtMyoE	GQ141545 - ACS35541.1
PtMyoF	GQ141546 - ACS35542.1
PtMyoG	GQ141547 - ACS35543.1
PtMyoH	GQ141548 - ACS35544.1
PtMyoI	GQ141549 - ACS35545.1
Actin-like proteins	*UniProt ID*
PtAct1	B7G878
PtAct2	B7G5C0

Name	Accession number
Myosins	*GenBank accession*
PtARP	B7G1C1
PtArp1	B5Y5B2
PtArp4	B7FWM6
PtArp4L	A0A8J9X9L0

Table 2. Myosin and actin-like proteins that we used in structural modeling.

For the myosin modeling, we individually aligned each of the *P. tricornutum* proteins with myosin-II from *Dictyostelium discoideum*, using the crystal structure bound to (-)-blebbistatin **[14]** (PDB ID: 3BZ7). We performed the alignments with Clustal W (https://www.genome.jp/tools-bin/clustalw) using the default settings for "fast/approximate" pairwise alignment (k-tuple (word) size: 1; window size: 5; gap penalty: 3; number of diagonals: 5; scoring method: percent). Based on the alignments, only the amino acid regions of each *P. tricornutum* myosin protein that aligned with the myosin-II structure from *D. discoideum* were selected for downstream model building. We built the structure models with Phyre one-to-one threading using 3BZ7 as the template, as well as the "local" alignment method, secondary structure scoring, and secondary structure weight of 0.1 (these are the default parameters that Phyre proposes). The confidence for all prepared structure models was 100% and the identity varied between 32% and 42%.

In preparation for the docking, we used Chimera and AutoDock Vina. We drew a box to encompass the position of the (-)-blebbistatin drug bound to the myosin-II structure from *D. discoideum* (PDB ID: 3BZ7). The position and dimensions of the box were: X center - 22.4025, Y center - 38.2512, Z center - 37.1841, X size - 14.1412, Y size - 8.04562, Z size - 12.4013. The box indicates the protein surface that should be explored for binding by the docking software. We used these coordinates for docking on the SwissDock web service (http://www.swissdock.ch). We used the blebbistatin molecule (Drugbank ID: DB07468) as the ligand. We used default docking parameters ("accurate" docking type and 0 angstrom flexibility for side chains). We also docked (-)-blebbistatin to the myosin-II structure (PDB ID: 3BZ7) to obtain an estimated delta G (kcal per mol) for a protein that's already empirically known to bind blebbistatin. For each docking result, we only used estimated delta G values for the top pose in our interpretations.

We modeled the CK-666 interaction with *P. tricornutum* and *Bos taurus* actins and actin-related proteins as described above, but based on the crystal structure of *B. taurus* Arp2 bound to CK-666 (PDB ID: 3UKR) **[15]**.

Actin activity predictions

We predicted *Phaeodactylum tricornutum* actin activity using published software **[16]**. Briefly, we fed the amino acid sequences of proteins identified as actin or actin-like proteins through the pipeline. This software uses sequence information to predict the proteins' ability to polymerize, ATPase activity, and similarity to actin.

Actin-binding protein homology

Below are the *Phaeodactylum tricornutum* proteins that we identified as actin-binding protein homologs with their accession numbers (Table 3).

Protein	Ensembl ID	UniProt ID
Cofilin	Phatr3_EG00210	B7FTG3
Tropomodulin	Phatr3_J47725	B7G4N9
DNase I	Phatr3_J35150	B7FXQ0
Gelsolin	Phatr3_J53980	B7FPI9
Villin	Phatr3_J45476	B7FXU1
Capping Protein	Phatr3_J35252	B7FXZ8
Capping Protein	Phatr3_J9601	B7FPL9
Formin	Phatr3_J54510	B7FZU7
Formin	Phatr3_J54229	B7FTV5
WASH	Phatr3_J46029	B7FZT7
Dynamin	Phatr3_J54751	B7G3L7
LSB3	Phatr3_Jdraft741	B7S483
LSB4/YSC84	Phatr3_J44183	B5Y5L8

Table 3. ***P. tricornutum*** **proteins that we identified as actin-binding protein homologs**.

The results

As described above, we are interested in understanding the determinants of morphotype specification in diatoms.

Serine endopeptidase induces *P. tricornutum* protoplast formation

To determine whether cells rely on the cell wall to maintain cell shape, we treated *P. tricornutum* UTEX646 cells with the commercial serine endopeptidase Alcalase, which was recently shown to effectively degrade the cell wall of the unicellular green algae *Chlamydomonas reinhardtii* **[17]**. To identify an optimal working concentration, we performed a concentration gradient ranging from 0.3 units/mL to 1.5 units/mL (Figure 3). After Alcalase treatment at 0.3 and 0.6 units/mL, we observed that 33–43% of cells formed protoplasts. When we treated cells with concentrations ≥1 Anson unit/mL, protoplasts were not visible, possibly due to excess cell death. Note that we only performed this gradient testing twice, and results from each trial are shown separately in Figure 3.

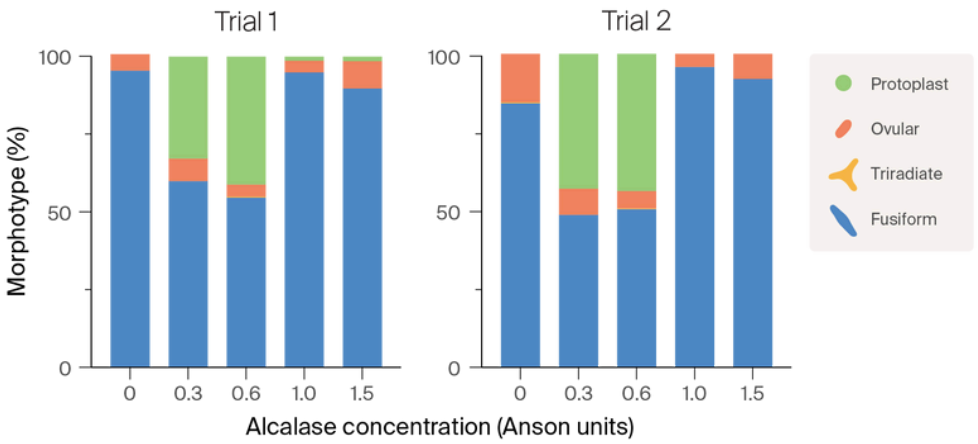

Figure 3

Enzyme concentration-dependent degradation of the *P. tricornutum* cell wall induces protoplast formation.

We treated UTEX646 cells with 0, 0.3, 0.6, 1.0, or 1.5 Anson units of Alcalase enzyme per mL of medium for 1 h at room temperature while rotating. *Note that we only performed this experiment twice, and each trial involved different cell growth conditions: in trial 1, we grew cells in Guillard's F/2 medium lacking silica, but they were in borosilicate flasks, which provide trace amounts of silica; in trial 2, we grew cells in standard Guillard's F/2 medium in borosilica

Video 1

Protoplast formation.

We treated *P. tricornutum* cells with 0.3 Anson units of Alcalase per milliliter of F/2 medium for 1 hour and then imaged them immediately without washing out the enzyme.

Additional live cell imaging revealed that these round cells were indeed protoplasts, as we observed them popping out of the fusiform cell wall (Video 1). These protoplasts remained viable for nearly two days without us washing them or exchanging the media (Video 2).

Video 2

Viable protoplasts after 40 hours.

We treated *P. tricornutum* cells with 0.3 Anson units of Alcalase per milliliter of F/2 medium for 1 hour and then immediately imaged them for 60 hours without washing out the enzyme. Internal dynamics are visible in protoplasts up to 40 hours after treatment.

Round *P. tricornutum* protoplasts attached to an “empty” fusiform cell wall were first described over half a century ago **[2]**. However, the authors noted an inability to observe the life cycle of these cells and did not provide any images. The strains used in the previous study were wild isolates now known as CCMP631 and the authors cite no difference in morphology between their isolate and other clonal isolates CCMP2557 and CCMP2559 (used in the present study; referred to as UTEX646), all of which take on a fusiform morphotype in >95% of cells **[13]**. Thus, it is likely that we’re observing the same phenomenon.

P. tricornutum strains have highly variable growth rates

We next hoped to see if these protoplasts were able to divide and reform the cell wall, and to see which morphotype(s) might then arise. While excited that we could observe viable protoplasts two days after induction, we were puzzled as to why we did not observe cell division under constant observation. Previous work reported that *P.*

tricornutum cells divide within 36–48 hours **[10][18][19]** and as early as within 13–19 hours in varied conditions **[18][20][21][22]**.

Since we did not observe protoplasts dividing within 50 hours of constant observation, we plotted the growth curves of two separate *P. tricornutum* strains over eight days (Figure 4). Surprisingly, we observed a doubling time of ~100 hours for UTEX646 and ~50 hours for CCMP2560, indicating that our imaging time was not nearly sufficient to observe the standard division rate of these cells.

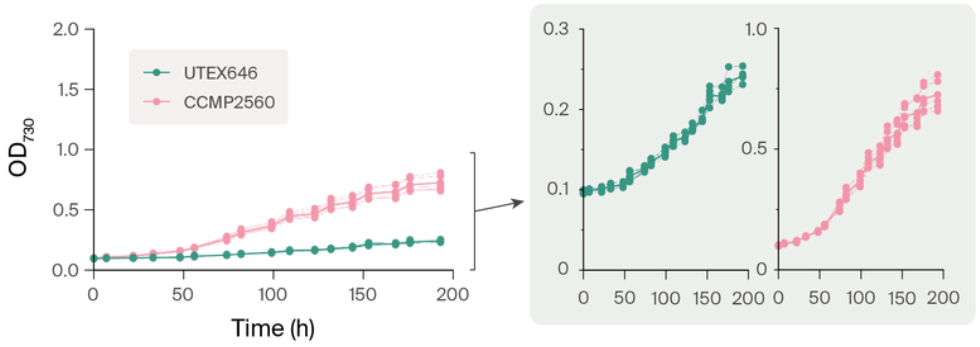

Figure 4

***P. tricornutum* division times are highly variable between strains**.

Optical density (OD) readings at a 730 nm absorbance wavelength over eight days. Right panel is the same data plotted with different y-axes to make slope changes clearer.

We could not observe cell division, so we continued investigating the role of the cell wall in maintaining cell morphology. We next wondered whether we'd still observe protoplast formation if we could disrupt the cell wall in a different, possibly gentler way.

Removing silica increases *P. tricornutum* protoplast formation

Diatoms incorporate silica into their cell walls; however, *P. tricornutum* is unique in its ability to survive in the absence of silica **[13]**. We decided to test whether growing *P.*

tricornutum without silica would disrupt the cell wall and again induce protoplast formation.

Silica crystals have been observed in water autoclaved in glass bottles **[23]** so we prepared silica-free media in polypropylene bottles and cultured cells in polypropylene Erlenmeyer flasks. We grew UTEX646 and CCMP2560 cells in media lacking silica, and then treated a fraction of cells with Alcalase enzyme and another fraction with glycerol as a vehicle control, since Alcalase is stored in a glycerol-containing buffer.

Interestingly, while UTEX646 cells grown in the presence of silica rarely formed protoplasts under control conditions ("Untreated" or "Glycerol"), these cells formed protoplasts more frequently when they grew without silica (Figure 5). Similarly, Alcalase-induced protoplasts were more frequent in silica-free cells.

CCMP2560 cells formed some protoplasts, independent of treatments or culture conditions (Figure 5). However, similar to UTEX646 cells, protoplasts formed much more frequently when we grew cells in the absence of silica (Figure 5). While silica is not essential for *Phaeodactylum* survival, these data demonstrate that it does contribute protoplast formation prevention.

Interestingly, for the experiments summarized in Figure 3, we grew cells for trial 1 in silica-free media autoclaved in borosilicate flasks. However, the rate of protoplast formation was nearly identical to trial 2, in which we grew cells in media that did contain silica, indicating that the trace presence of silica from glass bottles might be sufficient to impact the cell's ability to form protoplasts.

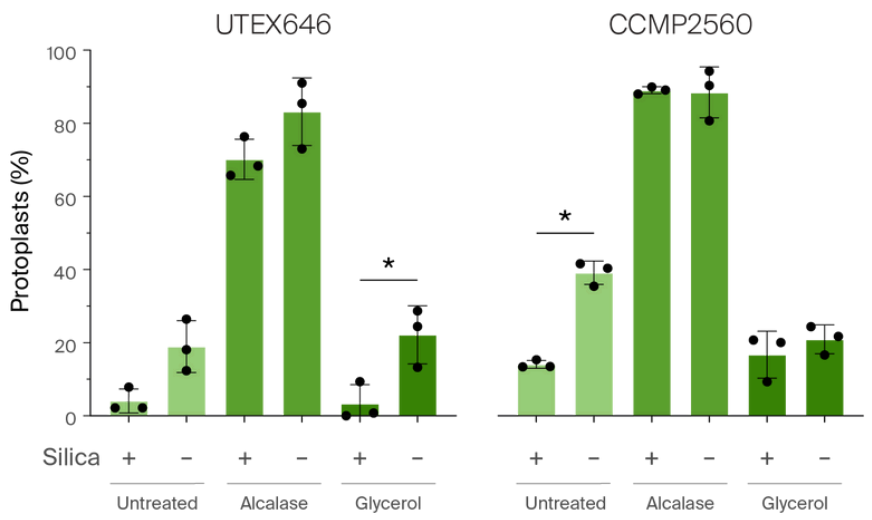

Figure 5

The absence of silica increases protoplast formation.

We grew UTEX646 and CCMP2560 cells in either standard Guillard's F/2 medium (+) or F/2-Si medium lacking silica (–). We treated cells with either additional media ("Untreated"), 0.3 units/mL Alcalase enzyme, or 5% glycerol because Alcalase is stored in glycerol solution. Data from three individual experiments. *$p < 0.05$.

Additional observations with a caveat

Treatment with drugs that inhibit the actin cytoskeleton alter its localization and induce protoplast formation

Finally, we wanted to probe the cytoskeleton's role in establishing and maintaining cell morphology. Pioneering work in *P. tricornutum* found that the filamentous actin (F-actin) cytoskeleton localizes to the cortex of the cell, near the cell wall **[9][10]**. To confirm that these are indeed functional actin networks and not aggregate stain stuck

near the cell wall, we treated UTEX646 cells with a panel of cytoskeletal drugs. These include the actin polymerization inhibitor latrunculin B; CK-666, an inhibitor of the branched actin-nucleating Arp2/3 complex; myosin II inhibitor (-)-blebbistatin; and the non-specific formin inhibitor SMIFH2.

We were unsuccessful in phalloidin-staining CCMP2560 cells so we only used the UTEX646 strain in further studies.

Treatment with each of these drugs altered phalloidin staining, which marks F-actin, suggesting that these are indeed F-actin networks (Figure 6). In control cells ("Untreated" and "2.5% DMSO"), we observed F-actin in dense networks along the cortex of the cell with some internal filamentous structures throughout. However, when we treated cells with latrunculin B, CK-666, or (-)-blebbistatin, the neatly organized filaments appeared to disassemble, leaving a cloudy cytoplasm and sparse puncta along the cell cortex, mainly at the very tip of the tapered fusiform cells.

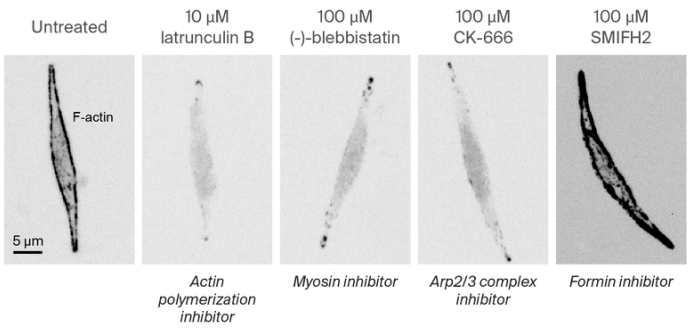

Figure 6

Inhibiting the cytoskeleton affects actin localization.

Representative images depict fixed UTEX646 cells stained with phalloidin-Atto 488 after a 2 hr treatment with the indicated drug.

Interestingly, cells that we treated with the formin inhibitor SMIFH2 appeared to have increased F-actin accumulation, both at the edge of the cells and with dense puncta throughout the cytoplasm. While initially identified as a formin inhibitor, recent work uncovered that this small molecule inhibitor is non-specific and also inhibits myosin activity **[24]**, making it difficult to interpret the effect of SMIFH2 on these cells.

Nonetheless, formin inhibition has been shown to increase Arp2/3 complex-mediated actin nucleation in yeast and mammalian cells **[25][26][27]**, but diatoms lack an Arp2/3 complex suggesting alternative mechanisms in these species **[5]**. Recent work using the plant model organism *Arabidopsis thaliana* discovered that joint inhibition of the Arp2/3 complex and formins increases the rate of *de novo* actin nucleation events **[28]**, possibly explaining our observations in formin-inhibited *P. tricornutum*.

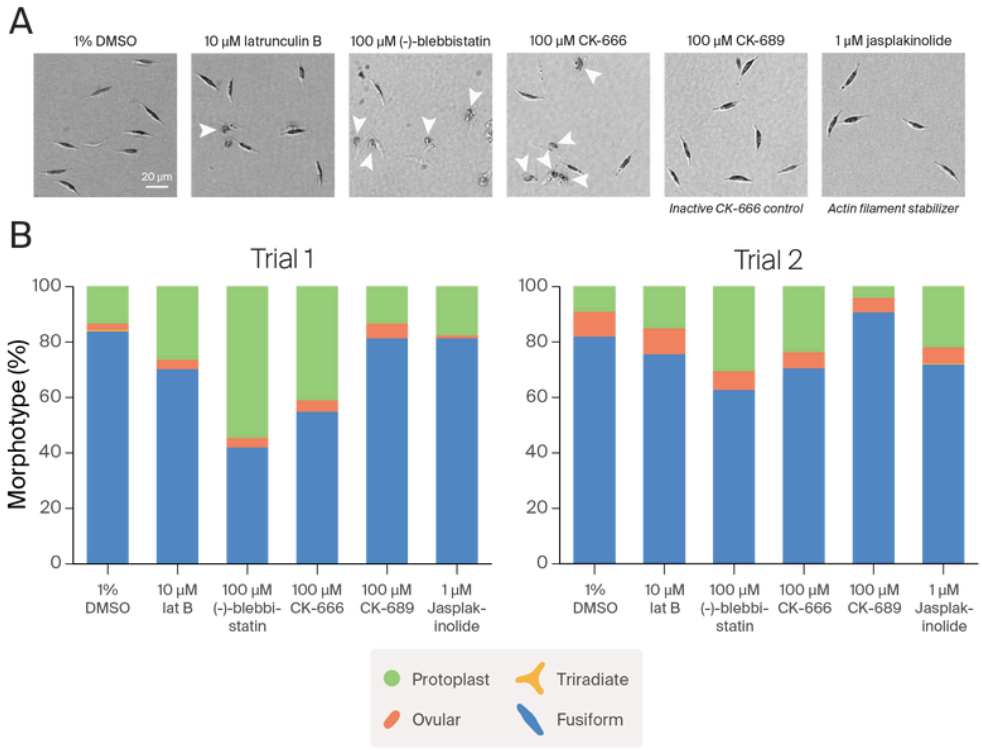

Figure 7

Cytoskeletal disruption induces protoplast formation in the diatom *P. tricornutum*.

A) Representative images of fixed UTEX646 cells that were not permeabilized or stained. Arrowheads indicate the presence of protoplasts.

B) Quantification of the percentage of cells from each morphotype. *Note that we show data from each of our first two experiments here — these trends did *not* repeat in subsequent testing.

Although we observed altered F-actin localization in the presence of these drugs, the cell morphology did not appear to be impacted (Figure 6), suggesting the actin cytoskeleton is not essential for maintaining cell shape. However, we noticed that some conditions had lower cell density than untreated cells and suspected our fixation technique might be causing cell death, so we decided to try a milder fixation protocol. We decided to move forward with just the drugs that appeared to disrupt F-actin assembly. We treated *P. tricornutum* cells with the indicated drugs for 2 hours, washed in fresh media, fixed in 4% paraformaldehyde, washed in 1× PBS, and then imaged them. We added the inactive CK-666 derivative CK-689 and the F-actin stabilizing jasplakinolide to this experiment as additional controls (Figure 7).

Caveat — Data not reproducible

We were only able to see protoplast formation after treatment with cytoskeletal drugs in our first two trials, presented in Figure 7. Subsequent attempts to replicate these findings resulted in 0% protoplast formation across treatments. Because we had not observed protoplasts forming in cells that had been permeabilized and stained, we thought our handling of the cells in subsequent trials might have been too harsh. To remedy this, we grew cells in 96 well plates and added the drugs directly to the media to a final concentration consistent with earlier trials. We imaged these cells overnight but were still unable to observe protoplasts forming.

Although unlikely, it is possible the light from the microscope inhibited the enzyme-induced protoplast egress, since we carried out previous treatments in the dark. Neither fresh media nor new drug stocks were able to recover the previous phenotype.

Possible avenues to explore that we did not pursue are media conditions (pH level; bespoke/purchased), cell cycle stage, and environmental conditions. Diatom researcher Nicole Poulsen suggested that we perform plasmolysis before cytoskeletal disruption after we shared these results on Twitter (thank you, Nicole!) and we agree that this would be a good idea to try; however, we've not yet followed up on this suggestion.

Keeping this caveat in mind, we present the results of our first two experimental trials here. Surprisingly, we observed an abundance of protoplasts forming in cells treated with actin cytoskeleton inhibitors (Figure 7).

We observed the most severe effect with the myosin II inhibitor (-)-blebbistatin, which led to around half of the cells becoming protoplasts. *P. tricornutum* has 10 different orphan myosin proteins **[29]**. Modeling based on the structure of (-)-blebbistatin bound to *Dictyostelium discoideum* myosin II **[14]**, suggests that this inhibitor is most likely to bind to myosin E, although it could bind to multiple *P. tricornutum* myosins (Figure 8 and Table 2). Thus, we can't definitively conclude which myosin or set of myosins is involved in preventing protoplast formation.

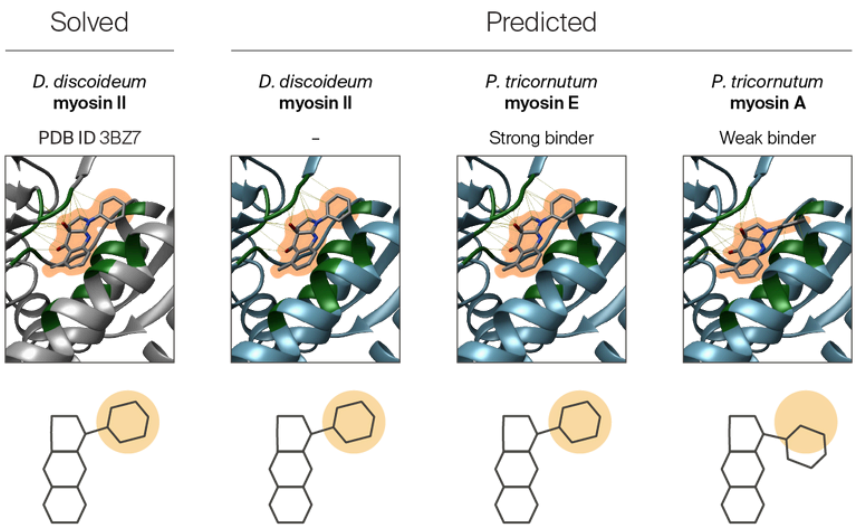

Figure 8

Predicted structural interactions between (-)-blebbistatin and *P. tricornutum* myosin.

The solved structure of *Dictyostelium discoideum* myosin II bound to (-)-blebbistatin (PDB: 3BZ7) is depicted on the left. The next three structures depict docking of (-)-blebbistatin on the Phyre-predicted structures of *D. discoideum* myosin II, *P. tricornutum* myosin E, and *P. tricornutum* myosin A, all based on PDB entry 3BZ7. Green indicates residues predicted to interact with the drug. Thin yellow lines indicate predicted protein–drug interactions. Orange silhouettes highlight the ligand. Skeleton drawings represent the orientation of the (-)-blebbistatin molecule when bound to myosin. Pale yellow circles highlight the clearest difference between predicted drug conformations.

Myosin	Predicted binding affinity (kcal/mol)	Protein length (aa)	Identity to *Dicty* myosin II	Fold change O–F*	Fold chang O–T
D. discoideum myosin II	-12.2	2116	–	–	
P. tricornutum Myo29	-9.5	2303	27%	–	-1.80323436
P. tricornutum MyoA	-3.4	1110	40%	3.827090363	4.46487593
P. tricornutum MyoB	-10.6	2016	32%	–	-2.53381016
P. tricornutum MyoC	-10.2	1157	40%	5.001125684	5.01180398
P. tricornutum MyoD	-10.5	1611	40%	–	-1.43462943
P. tricornutum MyoE	-11.4	1159	40%	1.317804061	1.91098406
P. tricornutum MyoF	-4.5	1488	37%	–	1.24833085
P. tricornutum MyoG	-10.1	1257	39%	–	
P. tricornutum MyoH	-10.3	1260	33%	–	
P. tricornutum MyoI	-10.3	1634	38%	-1.329124352	-1.76816

Table 4. Based on structural modeling with an orthologue, blebbistatin is most likely to bind *P. tricornutum* MyoE. We obtained predicted binding affinities using

Chimera and AutoDock Vina, as described under "Modeling and docking." Percent identity represents how identical the *Phaeodactylum* myosin amino acid sequences are to the *Dictyostelium discoideum* myosin II amino acid sequences. *Ovide and colleagues **[3]** determined the values in these columns experimentally. O–F indicates a comparison of ovular cells to fusiform cells. O–T indicates a comparison of ovular cells to triradiate cells. A positive value indicates expression is upregulated in ovular cells and a negative value indicates expression is downregulated in ovular cells. Values indicate the RNA-Seq log2 fold change.

—

We observed the next-most severe effects in cells treated with the Arp2/3 complex inhibitor CK-666 (Figure 7). As expected, treatment with the inactive CK-666 derivative, CK-689, was indistinguishable from treatment with DMSO. CK-666 binds to the Arp2 subunit of the Arp2/3 complex, preventing the conformational change needed to activate the Arp2/3 complex, thereby inhibiting the nucleation of branched actin filaments **[15]**. Strangely, *P. tricornutum* cells and other diatoms do not express homologs to the Arp2/3 complex subunits **[5]**, so it's unclear why this drug would have such a strong effect.

We speculate that this small molecule inhibitor could be binding and inhibiting another actin-related protein in *P. tricornutum*. Since the interaction between CK-666 and *Bos taurus* Arp2 is solved **[15]**, we were able to model the interactions between CK-666 and the six actin and actin-related *P. tricornutum* proteins. Although the binding affinities were relatively similar across predictions (Table 3), the orientation of the drug in the binding pocket appears to be most similar between *B. taurus* Arp2 and *P. tricornutum* Act1 and Act2 (left column), while the orientation of CK-666 bound to *B. taurus* actin looks quite different (top-right image) (Figure 9). Further, we used recently published actin family prediction software which supports the assumption that Act1 and Act2 are the only polymerizable, enzymatic actin proteins in *P. tricornutum* (Table 3) **[16]**. These data suggest that the CK-666 function and mechanism of action are not consistent across species and indicate that the drug could be inhibiting actin polymerization in these diatoms.

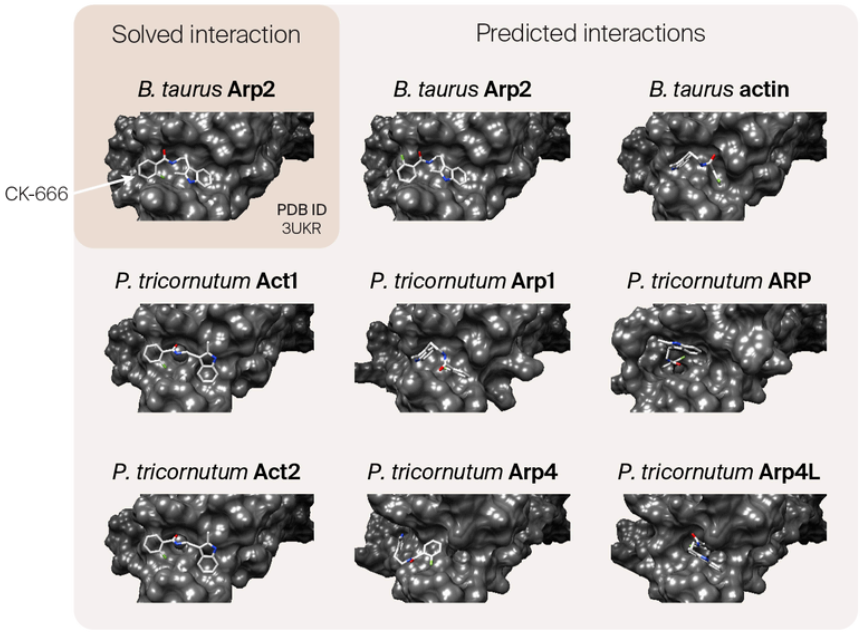

Figure 9

Predicted structural interactions between CK-666 *P. tricornutum* actin and actin-related proteins.

The solved structure of *Bos taurus* Arp2 bound to CK-666 (PDB: 3UKR) is on the top-left. The remaining structures depict docking of CK-666 on the Phyre-predicted structures of *B. taurus* Arp2 and Actin and *P. tricornutum* proteins Act1, Act2, Arp1, ARP, Arp4, and Arp4L, all based on PDB entry 3UKR.

Protein	Predicted binding affinity (kcal/mol)	Protein length (amino acids)	Identity to *B. taurus* Arp2	Longi-tudinal polymeri-zation*	Lati-tudinal polymeri-zation*	ATP acti
B. taurus Arp2	-7.1	394	-	-	-	
B. taurus actin, cytoplasmic 1	-6.2	375	62%	-	-	
P. tricornutum Act1	-6.2	377	61%	82%	100%	

Protein	Predicted binding affinity (kcal/mol)	Protein length (amino acids)	Identity to *B. taurus* Arp2	Longi-tudinal polymeri-zation*	Lati-tudinal polymeri-zation*	ATP acti
P. tricornutum Act2	-6.2	377	61%	82%	100%	
P. tricornutum Arp1	-5.6	391	54%	56%	57%	
P. tricornutum ARP	-6.6	463	28%	26%	29%	
P. tricornutum Arp4	-5.4	523	22%	38%	29%	
P. tricornutum Arp4L	-6.1	484	21%	38%	14%	

Table 5. Based on structural modeling with an ortholog, CK-666 is more likely to bind predicted *P. tricornutum* actins Act1 and Act2 than its homologs. We obtained predicted binding affinities for CK-666 with various known and potential cytoskeletal proteins using Chimera and AutoDock Vina, as described under "Modeling and docking." Percent identity represents how identical the *Phaeodactylum* protein sequences are to the *Bos taurus* Arp2 amino acid sequences — similar structures could be more likely to bind CK-666. Longitudinal polymerization, latitudinal polymerization, and ATPase activity percentages represent the percent of residues required for the indicated function present in the query protein — these are key functions of actin, so the higher values for PtAct1 and PtAct2 suggest these are functional actins. Percent actin identity is based on the protein sequence identity between the target protein and a multiple sequence alignment of several well-studied actin proteins — this is another key clue that PtAct1 and PtAct2 are indeed true actins.

—

Key takeaways

- The serine endopeptidase Alcalase induces protoplast formation.
- Protoplast formation is more frequent in the absence of silica.
- Trace amounts of silica from glassware may be sufficient to prevent protoplast formation.
- Cell division times are drastically different between strains of the same species.
- Some drugs, specifically CK-666, aren't reliable across species.
- Actin and myosin may contribute to the prevention of protoplast formation, possibly by trafficking cell wall components (caveat — this conclusion is based on initial findings that we could not consistently reproduce.)

Possible follow-up work

While these experiments provide novel insights into diatom morphologies and contributions of the actin cytoskeleton, there are many more experiments that would allow us to better understand these processes. **Our focus has shifted to other projects, so we are not currently pursuing the follow-up experiments described in this section**. We encourage members of the community to run with these ideas! Please reach out if you plan to continue this project, as we would love to follow your progress! If we decide to return to these experiments, we will comment on or update this pub.

First, it will be important to understand why we saw inconsistent results with our cytoskeletal drug treatments. As explained, two initial trials showed protoplast formation, but we saw no protoplasts in subsequent trials. There are several parameters that could be adjusted to optimize this sensitive assay. In our initial experiments, we did not carefully control the environmental conditions and kept cells growing at ambient temperature, which fluctuates throughout the day and season. Further, we switched from making bespoke F/2 medium to purchasing F/2 medium (UTEX) to ensure consistent quality; however, we didn't carefully note the source of the media in each experiment or do a thorough comparison of pH differences between media. Finally, the cells were not synchronized and since we observed a ~100-hour

doubling time, it's unlikely the cells were in the same phase of the cell cycle across experiments.

Additional attempts to test these results could benefit from culturing the cells at a consistent temperature, adjusting the pH or components of the growth medium, and synchronizing the cells. However, the cells used in other, replicable experiments were maintained in the same manner, so it is unclear if these factors will matter.

It would be interesting to observe the fate of the protoplasts we observe after Alcalase treatment or growth without silica and to see what happens when they divide and form new cell walls, especially while their cytoskeleton is disrupted by drugs in the media, but the long division time for this diatom has made such an experiment difficult. An alternative method would be to knock out actin-nucleating proteins through modern gene-editing techniques, such as CRISPR, which others have established in *P. tricornutum* **[30][31][32]**. However, cell wall reassembly may not occur while the actin cytoskeleton is inhibited, since previous work revealed treatment with the actin polymerization inhibitor cytochalasin D prevents protoplast reversion in the cell-walled yeast species *Schizosaccharomyces pombe* **[33]**.

Additionally, our observations indicate that cytoskeletal inhibitors and the serine endopeptidase Alcalase have similar impacts on protoplast formation. Future studies might determine whether Alcalase has any negative effects on actin nucleation or polymerization. This could be tested by observing the impact of the enzyme on actin-dependent functions in another species lacking a cell wall. Alternatively, one could perform biochemical actin polymerization assays with purified actin in the presence or absence of Alcalase. That said, the enzyme is suspended in glycerol, which may impact these sensitive assays.

We saw protoplast formation when we treated cells with the myosin inhibitor (-)-blebbistatin. There is precedent suggesting that altered expression of *P. tricornutum* myosins contributes to cell morphology. Previous studies indicated that myosins A, C, E, and F are expressed at higher levels in fusiform or triradiate morphotypes compared to ovular cells, while myosins B, D, I, and 29 are downregulated **[3]**. As mentioned previously, ovular cells have trackable gliding motility **[11]**, similar to the actin-dependent motility reported in another pennate diatom, *Craspedostauros australis* **[12]**, suggesting myosins B, D, I, and/or 29 could be contributing to cell motility. However, in response to increased copper availability, a similar pennate diatom *Mayamaea pseudoterrestris* increases both gliding speed and the expression of

myosins A, C, and E **[34]**. Interestingly, myosins A, C, E, G and I appear to be exclusively expressed in pennate diatom species, while B, D, F, H, and 29 are also found in non-gliding radially symmetric centric diatoms **[34]**. It would be fascinating to see further studies characterizing the functions of these “orphan” myosins.

Finally, we have generated preliminary data using the SPY555-FastAct dye to image live actin dynamics. This work revealed structures similar to Arp2/3 complex-nucleated endocytic actin patches (Video 3) **[35]**. Although *P. tricornutum* expresses several components of the endocytic machinery, it is unclear if these cells can form branched actin networks or not. Platinum replica electron microscopy could help identify whether these are indeed branched actin networks. If so, given the absence of Arp2/3 complex subunits, this system could be pivotal in identifying Arp2/3 complex-independent mechanisms of branched actin assembly or the presence of divergent Arp2/3 complex subunits not identifiable by sequence alone.

Video 3

Dynamic, cortical actin puncta.

SPY555-FastAct-stained CCMP2560 cells grown with or without silica.

Left column: Silica present

Right column: Silica absent

Top row: Triradiate morphotype

Bottom row: Fusiform morphotype

Interestingly, in the limited number of movies that we recorded, the dynamics of these puncta are substantially different between cells grown in the presence or absence of

silica (Video 3, left vs. right columns). Recent work has provided substantial evidence that the presence of silica nanoparticles impacts actin properties and functions **[36] [37]**. It is unclear if the altered *P. tricornutum* actin puncta dynamics are caused by differences in the cell wall or if the presence of silica is physically altering actin dynamics.

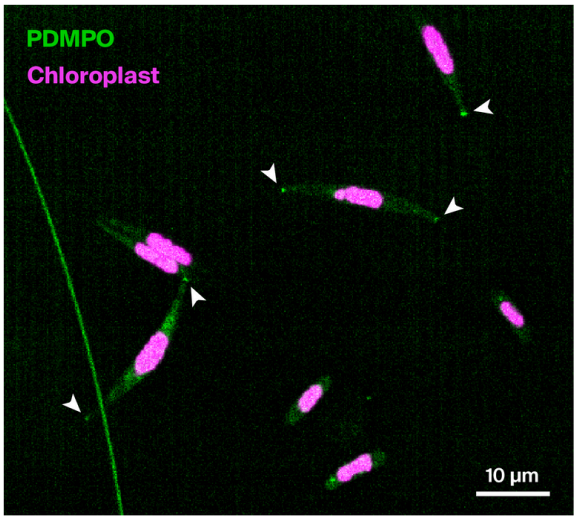

Figure 10

Silica localization in fusiform cells.

Silica staining with PDMPO (green) and chloroplast autofluorescence (magenta). Arrowheads indicate the presence of PDMPO staining. The curved, green line is an artifact from the microscope.

These experiments can be expanded and improved upon using genetically engineered *P. tricornutum* cells expressing a fluorescent cytoskeletal marker, such as LifeAct-GFP, reducing cell-to-cell signal variability that is inherent with dyes. Notably, our preliminary attempts to visualize the localization of silica deposits in *P. tricornutum* using PDMPO (a fluorescent probe for silica deposition) indicate dense silica puncta present at the tips of fusiform cells (Figure 10) **[38]**. These puncta are reminiscent of the residual actin staining observed after treatment with cytoskeletal inhibitors in Figure 6, and would be an interesting topic to explore further. Alternatively, these cortical tips might just be more prone to taking up non-specific dyes. Importantly,

previous attempts to visualize silica deposits in *P. tricornutum* using LysoTracker™ HCK-123 dye and FITC-silane did not follow this pattern in fusiform or ovular cells **[39]**. While we are not currently pursuing these leads, we are excited about the potential findings these experiments could uncover.

References

1. He L, Han X, Yu Z. (2014). A Rare Phaeodactylum tricornutum Cruciform Morphotype: Culture Conditions, Transformation and Unique Fatty Acid Characteristics. https://doi.org/10.1371/journal.pone.0093922

2. Lewin JC, Lewin RA, Philpott DE. (1958). Observations on Phaeodactylum tricornutum. https://doi.org/10.1099/00221287-18-2-418

3. Ovide C, Kiefer-Meyer M-C, Bérard C, Vergne N, Lecroq T, Plasson C, Burel C, Bernard S, Driouich A, Lerouge P, Tournier I, Dauchel H, Bardor M. (2018). Comparative in depth RNA sequencing of P. tricornutum's morphotypes reveals specific features of the oval morphotype. https://doi.org/10.1038/s41598-018-32519-7

4. Kollmar M, Lbik D, Enge S. (2012). Evolution of the eukaryotic ARP2/3 activators of the WASP family: WASP, WAVE, WASH, and WHAMM, and the proposed new family members WAWH and WAML. https://doi.org/10.1186/1756-0500-5-88

5. Aumeier C, Polinski E, Menzel D. (2015). Actin, actin-related proteins and profilin in diatoms: A comparative genomic analysis. https://doi.org/10.1016/j.margen.2015.07.002

6. Pollard TD, Cooper JA. (2009). Actin, a Central Player in Cell Shape and Movement. https://doi.org/10.1126/science.1175862

7. Fletcher DA, Mullins RD. (2010). Cell mechanics and the cytoskeleton. https://doi.org/10.1038/nature08908

8. Luxenburg C, Zaidel-Bar R. (2019). From cell shape to cell fate via the cytoskeleton — Insights from the epidermis. https://doi.org/10.1016/j.yexcr.2019.03.016

9 Galas L, Burel C, Schapman D, Ropitaux M, Bernard S, Bénard M, Bardor M. (2021). Comparative Structural and Functional Analyses of the Fusiform, Oval, and Triradiate Morphotypes of Phaeodactylum tricornutum Pt3 Strain. https://doi.org/10.3389/fpls.2021.638181

10 Tanaka A, De Martino A, Amato A, Montsant A, Mathieu B, Rostaing P, Tirichine L, Bowler C. (2015). Ultrastructure and Membrane Traffic During Cell Division in the Marine Pennate Diatom Phaeodactylum tricornutum. https://doi.org/10.1016/j.protis.2015.07.005

11 Iwasa K, Shimizu A. (1972). Motility of the diatom, Phaeodactylum tricornutum. https://doi.org/10.1016/0014-4827(72)90416-8

12 Poulsen NC, Spector I, Spurck TP, Schultz TF, Wetherbee R. (1999). Diatom gliding is the result of an actin-myosin motility system. https://doi.org/https://doi.org/10.1002/(SICI)1097-0169(199909)44:1<23::AID-CM2>3.0.CO;2-D

13 Martino AD, Meichenin A, Shi J, Pan K, Bowler C. (2007). Genetic and phenotypic characterization of *Phaeodactylum tricornutum* (Bacillariophyceae) accessions[1]. https://doi.org/10.1111/j.1529-8817.2007.00384.x

14 Lucas-Lopez C, Allingham JS, Lebl T, Lawson CPAT, Brenk R, Sellers JR, Rayment I, Westwood NJ. (2008). The small molecule tool (S)-(–)-blebbistatin: novel insights of relevance to myosin inhibitor design. https://doi.org/10.1039/b801223g

15 Baggett AW, Cournia Z, Han MS, Patargias G, Glass AC, Liu S, Nolen BJ. (2012). Structural Characterization and Computer-Aided Optimization of a Small-Molecule Inhibitor of the Arp2/3 Complex, a Key Regulator of the Actin Cytoskeleton. https://doi.org/10.1002/cmdc.201200104

16 Avasthi P, Bigge BM, Reiter T. (2024). Defining actin: Combining sequence, structure, and functional analysis to propose useful boundaries. https://doi.org/10.57844/ARCADIA-YNTH-KH70

17 Hwang H-J, Kim YT, Kang NS, Han JW. (2018). A simple method for removal of the Chlamydomonas reinhardtii cell wall using a commercially available subtilisin (Alcalase). https://doi.org/10.1159/000495183

18 Heydarizadeh P, Veidl B, Huang B, Lukomska E, Wielgosz-Collin G, Couzinet-Mossion A, Bougaran G, Marchand J, Schoefs B. (2019). Carbon Orientation in the Diatom Phaeodactylum tricornutum: The Effects of Carbon Limitation and Photon Flux Density. https://doi.org/10.3389/fpls.2019.00471

19 Zhao P, Gu W, Wu S, Huang A, He L, Xie X, Gao S, Zhang B, Niu J, Peng Lin A, Wang G. (2014). Silicon enhances the growth of Phaeodactylum tricornutum Bohlin under green light and low temperature. https://doi.org/10.1038/srep03958

20 Mann JE, Myers J. (1968). ON PIGMENTS, GROWTH, AND PHOTOSYNTHESIS OF *PHAEODACTYLUM TRICORNUTUM*[12]. https://doi.org/10.1111/j.1529-8817.1968.tb04707.x

21 Greene RM, Geider RJ, Kolber Z, Falkowski PG. (1992). Iron-Induced Changes in Light Harvesting and Photochemical Energy Conversion Processes in Eukaryotic Marine Algae. https://doi.org/10.1104/pp.100.2.565

22 D'Elia CF, Guillard RRL, Nelson DM. (1979). Growth and competition of the marine diatoms Phaeodactylum tricornutum and Thalassiosira pseudonana. I. Nutrient effects. https://doi.org/10.1007/bf00387007

23 Lohmiller J, Lipman N. (1998). Silicon crystals in water of autoclaved glass bottles

24 Nishimura Y, Shi S, Zhang F, Liu R, Takagi Y, Bershadsky AD, Viasnoff V, Sellers JR. (2021). The formin inhibitor SMIFH2 inhibits members of the myosin superfamily. https://doi.org/10.1242/jcs.253708

25 Murugesan S, Hong J, Yi J, Li D, Beach JR, Shao L, Meinhardt J, Madison G, Wu X, Betzig E, Hammer JA. (2016). Formin-generated actomyosin arcs propel T cell receptor microcluster movement at the immune synapse. https://doi.org/10.1083/jcb.201603080

26 Rotty JD, Wu C, Haynes EM, Suarez C, Winkelman JD, Johnson HE, Haugh JM, Kovar DR, Bear JE. (2015). Profilin-1 Serves as a Gatekeeper for Actin Assembly by Arp2/3-Dependent and -Independent Pathways. https://doi.org/10.1016/j.devcel.2014.10.026

27 Burke TA, Christensen JR, Barone E, Suarez C, Sirotkin V, Kovar DR. (2014). Homeostatic Actin Cytoskeleton Networks Are Regulated by Assembly Factor Competition for Monomers. https://doi.org/10.1016/j.cub.2014.01.072

28 Xu L, Cao L, Li J, Staiger CJ. (2022). Cooperative actin filament nucleation by the Arp2/3 complex and formins maintains the homeostatic cortical array in Arabidopsis epidermal cells. https://doi.org/10.1101/2022.08.03.502536

29 Heintzelman MB, Enriquez ME. (2010). Myosin diversity in the diatom *Phaeodactylum tricornutum*. https://doi.org/10.1002/cm.20431

30 Nymark M, Sharma A, Hafskjold M, Sparstad T, Bones A, Winge P. (2017). CRISPR/Cas9 Gene Editing in the Marine Diatom Phaeodactylum tricornutum. https://doi.org/10.21769/bioprotoc.2442

31 Stukenberg D, Zauner S, Dell'Aquila G, Maier UG. (2018). Optimizing CRISPR/Cas9 for the Diatom Phaeodactylum tricornutum. https://doi.org/10.3389/fpls.2018.00740

32 Slattery SS, Diamond A, Wang H, Therrien JA, Lant JT, Jazey T, Lee K, Klassen Z, Desgagné-Penix I, Karas BJ, Edgell DR. (2018). An Expanded Plasmid-Based Genetic Toolbox Enables Cas9 Genome Editing and Stable Maintenance of Synthetic Pathways in *Phaeodactylum tricornutum*. https://doi.org/10.1021/acssynbio.7b00191

33 Kobori H, Yamada N, Taki A, Osumi M. (1989). Actin is associated with the formation of the cell wall in reverting protoplasts of the fission yeast *Schizosaccharomyces pombe*. https://doi.org/10.1242/jcs.94.4.635

34 Suzuki S, Ota S, Yamagishi T, Tuji A, Yamaguchi H, Kawachi M. (2022). Rapid transcriptomic and physiological changes in the freshwater pennate diatom*Mayamaea pseudoterrestris*in response to copper exposure. https://doi.org/10.1093/dnares/dsac037

35 Goode BL, Eskin JA, Wendland B. (2015). Actin and Endocytosis in Budding Yeast. https://doi.org/10.1534/genetics.112.145540

36 Ispanixtlahuatl-Meráz O, Schins RPF, Chirino YI. (2018). Cell type specific cytoskeleton disruption induced by engineered nanoparticles. https://doi.org/10.1039/c7en00704c

37 Cornu R, Chrétien C, Pellequer Y, Martin H, Béduneau A. (2020). Small silica nanoparticles transiently modulate the intestinal permeability by actin cytoskeleton disruption in both Caco-2 and Caco-2/HT29-MTX models. https://doi.org/10.1007/s00204-020-02694-6

38 Shimizu K, Del Amo Y, Brzezinski MA, Stucky GD, Morse DE. (2001). A novel fluorescent silica tracer for biological silicification studies. https://doi.org/10.1016/s1074-5521(01)00072-2

39 Desclés J, Vartanian M, El Harrak A, Quinet M, Bremond N, Sapriel G, Bibette J, Lopez PJ. (2007). New tools for labeling silica in living diatoms. https://doi.org/10.1111/j.1469-8137.2007.02303.x